RANDOM VIBRATIONS IN COMPLEX ELECTRONIC STRUCTURES

Alson E. Hatheway

MSC/NASTRAN User's Conference
March 24-25, 1983
Huntington-Sheraton Hotel
Pasadena, California

Alson E. Hatheway, Incorporated
Consulting Engineers
1041 East Green Street
Pasadena, CA 91106
(213) 795-0514

ABSTRACT

Finite element methods can predict the stresses and strains in complex electronic structures. The accuracy of the results are effected by the modeling strategy used and the distribution of mass, stiffness and damping in the structure. Mass and stiffness are distributed during the normal modeling procedure of defining geometry, elements and materials. Damping, however, is usual distributed "uniformly" through the model or sometimes specified as a function of frequency, as in modal damping. Various damping distributions have been explored with the use of material damping entered on the MAT1 card. The redistribution of material damping has been found to influence the computational results and some combinations of material damping have substantially improved the correlation between MSC/NASTRAN analysis and random vibration test data.

INTRODUCTION

AEH is involved in the design and development of complex electronic systems for use in severe environments. The present work is an extension of earlier work at AEH to correlate random vibration test data that was obtained during test of complex printed wiring board assemblies. Significant improvements in the accuracy of the computations have been made. It is hoped that these results will lead to reliable modeling strategies for electronic assemblies.

TESTS

The test specimen of interest in this study is shown in Figure 1. It consists of an eight layer polyimide printed wiring board (PWB) with copper ground planes bonded to both sides. The PWB carries a combination of discrete capacitors, leadless chip carriers (LCC), and ceramic substrates. The substrates in turn carry arrays of LCCs soldered to them. Along one edge of the assembly is a multi-pin input/output connector. The opposite edge carries an aluminum stiffener with integral test points. The free edges are used to install the PWB into its chassis with Wedge-Lok type clamps. The entire speciment weighs .73 pounds. Composition of the assembly's parts is shown in Table I. All of the electronic piece parts are attached to the PWB and substrate by lead-tin solder. Additionally, the phospher bronze pins are soldered to both the PWB and substrates. All of the exposed copper and bronze surfaces are solder coated.

The test specimen was mounted in a ridged fixture for the test. The fixture was made from one inch thick aluminum tooling plate with holes which matched the armature of the shaker head. The fixture attached to the shaker can be seen in Figure 1 and Figure 2. The test specimen is installed in the fixture by sliding the edges of the specimen into slots machined in the fixture. When the speciment is longitudinally centered in the slots, the specimen is secured by tightening the Wedge-Lok devices.

Figures 1 and 2 also show the central accelerometer and three of the four strain gauges attached to the specimen. The fourth strain gauge is not visible since it is on the far side of the PWB opposite the accelerometer. The central accelerometer is shown attached to the fixture near the slot which receives one edge of the specimen.

With the specimen, fixture and instrumentation thus installed on the shaker, the specimen was exposed to vibrations normal to the plain of the specimen.

The test program included a 5g sine wave from 100 to 2,000 Hz. followed by random vibrations. The random vibrations were begun at $.01g^2$/Hz. from 100 to 2,000 Hz. with a five minute dwell after equalization. Subsequently, the PSD level was increased to $.40g^2$/Hz. for five minutes and then finally to $1.6g^2$/Hz. After 1.5 minutes at $1.6g^2$/Hz. the specimen fractured.

The test specimen was instrumented with one central accelerometer and four resistance strain gauges. The locations are shown in Figure 3. The responses to the random vibrations of various levels are shown in Table II. Significant resonant frequencies were observed at 265 Hz., 495 Hz. and 1,220 Hz. (by the accelerometer). These frequencies were seen to drop about 20% as the test level was increased from $.01g^2$/Hz. to $1.60g^2$/Hz. Obviously, some non-linear effects are displayed in the test data. It was decided to attempt to correlate the data at one drive level and assume that if this were successful, the other levels could be similarly correlated by adjusting the model parameters (damping and stiffness).

The fractured specimen is shown in Figure 4. The failure process began with separation of chip carrier packages from both the PWB and substrates. At the same time, solder pins were observed to be cracking loose from the assembly. The process culminated with the fracture of two substrates, at which time the test was terminated. The above failure phenomena were observed to follow in very rapid succession just prior to test termination.

ANALYSIS

The analysis attempts to corroborate the test results. Since normal qualification tests run about 30 minutes per axis, and fatigue strength varies roughly as the -3.3 power of test time, it was felt that the $.40g^2$/Hz. test level was a reasonably severe environment in which to attempt to correlate the test data. This is the level that was used throughout the subsequent analytical investigation. The analysis spectrum was from 100 to 2,000 Hz. and all eigenvalues in this range were entered on a FREQ card (approximately 23 frequencies). Additional frequencies were selected on a FREQ1 card (four intervals between 100 Hz. and 200 Hz.) and a FREQ2 card (100 intervals between 200 Hz. and 2,000 Hz.). In all, approximately 128 intervals were used between 100 Hz. and 2,000 Hz. for integrating to determine the RMS responses.

The computation procedures used were SOL 71 for Modal Random Response and SOL 63 used to obtain mode shapes and modal strain energies. The super element sequences were used because during later portions of the analysis, it was possible (with an alter) to restart the problem in SOL 71 with changes to G on the MAT1 cards and not have to rerun the eigenvalue extraction portion of the problem. Since a large number of "damping restarts" were made, considerable computer time was saved using this procedure. A sample Executive Control Deck is shown in Figure 5 with the alter and notes on its use included.

The structural model is shown in Figure 3. It is composed of shell and bar elements with a mesh size intended to give a minimum of five elements per wave length of mode. The constraints and supports are modeled so the assembly can be excited along the axis normal to the plane of the PWB (Z axis).

The effects of several modeling variations have been explored. Originally, the substrate solder pins were modeled as orthotropic shell elements attaching the perimeter of each substrate to the PWB. Straight bar elements were substituted for the shell elements. Then the straight bar elements were replaced with bent bar elements which accurately reflected the geometry of the solder pins themselves. Each of these configurations was evaluated.

Additionally, the shape of a few shell elements was adjusted so that element center would more accurately represent the measured location of the strain gauges on the test specimen. The changes made are visible in Figure 6. A summary of these modeling effects is shown in Table III with all data normalized to the test data accelerometer response. The modeling variations tend to increase the strain calculated at locations 01, 02, and 04, while leaving the strain a location 03 nearly unchanged. Although these variations did not improve the correlation with the test data, each of the variations was felt to be an improvement on the model which should produce more accurate computational results and, therefore, they were left in the model for the subsequent investigations of material properties.

MATERIAL PROPERTIES

Initially, there was uncertainty about the appropriate values to use for the Young's Modulus of the polyimide PWB and the ceramic substrates. The flexural properties of the PWB are a combination of the polyimide/glass fiber layers, the copper conduction inner layers, the copper ground plane outer layers and the lead-tin solder coating applied to all exposed copper surfaces of the PWB. When the plate properties of the MSC/NASTRAN model were adjusted to resemble the as-built configuration of the test specimen the fundamental mode was within 10% of the test value, so it was not felt to be necessary to deviate from handbook values of the properties of this material.

On the other hand, the value of Young's Modulus for the alumina ceramic is not well established. Quoted values vary from 25 million to 50 million pounds per square inch, depending upon purity of the material. But even in one purity grade the modulus may vary widely. It is even reported that test specimens cut from different parts of the same sheet will show large variations. In general, specifications for electronics grade alumina do not specify Young's Modulus and it is therefore not a controlled parameter.

Several computational runs were made to determine what value of Young's Modulus for alumina would best corroborate the test data. Values of the modulus between 20 million and 50 million pounds per square inch were used. Over this range, the lowest eigenvalue associated with large displacements in the substrates varied from 960 Hz. to 1,700 Hz. so that Young's Modulus has a pronounced influence on the frequency of the resonant peak observed at 1,220 Hz. during the tests.

The RMS value of strain at the location of the four strain gauges showed a net variation of about 10% (plus or minus 5%) while Young's Modulus was varied over its full range. A value of 38.9 million pounds per square inch, a value quoted for 94% pure microelectronics grade alumina, gave reasonable results with the resulting high frequency resonance at 1,079 Hz. This value was used in subsequent computations.

With the model geometry and material elastic properties now established it was necessary to evaluate the influence of damping distribution on the computational results. Damping was specified by entering a value for G, structural damping, in field 9 of the MAT1 cards. All materials with blanks or zeros in field 9 will have no damping. It is therefore possible to distribute damping to discrete portions of the model. By making several computational runs with damping entered on different MAT1 cards, it is possible to observe the influence of changes in damping distribution

on the response of the model. The alter discussed earlier was very useful by facilitating these runs as restarts.

Several areas of the test specimen could have significantly higher damping than others. These include the PWB, the solder pins, the Wedge-Loks, the test connector and the card connector. Damping was applied to the model via the MAT1 cards to simulate high local damping in each of the above areas. The damping value was adjusted to give about the same accelerometer response as the test data and the results were normalized to the accelerometer. The results are compared to the test data in Table IV. Applying damping to the card connector elements gave the best corroboration of the test data. Appying damping to two places simultaneously was run and two of these results are shown also in Table IV. No combination of two or more damping locations was found which agreed with the test data as well as applying the damping only to the card connector.

DISCUSSION

Early concerns about the influence of Young's Modulus on the computation results are not validated. Although resonant frequencies (and eigenvalues) respond as anticipated to this variable, the overall influence on RMS acceleration and strain responses is slight. This does not imply that Young's Modulus is unimportant in interpreting the results. In estimating the accumulated fatigue damage caused by random vibration, most analyst use a form of Miner's Rule which counts the number of load cycles (which is proportional to frequency) and therefore stiffness is important. Furthermore, fatigue behavior in materials is specified in the stress domain, not the strain domain, and therefore a factor of two variation in Young's Modulus may result in factors of eight or ten variation in fatigue life, for the same computed strain value.

Random vibration data is some of the most difficult to correlate with linear theory. Comparison of the random response and sine response curves of Figure 7 is instructive. The resonant peak at 1,220 Hz. which is sharply defined in the sine response curve shows a significant attenuation in the random response curve. Additionally, the deep trough between 500 Hz. and 1,000 Hz. in the sine response curve is substantially filled in the random response curve. It is probable that the card extractor levers were loose enough to rattle during the tests. This effect tended to reduce the response at 1,220 Hz. and distribute the energy across the spectrum, where it shows up in the valley during random tests. However, since the sine wave response records all the energy at only the frequency of excitation it appears to be a much cleaner response curve, even though the rattling was occurring there also. Comparing the two test curves of Figure 7 to the typical MSC/NASTRAN response curve of Figure 8, it is clear that the sine response curve more nearly resembles the MSC/NASTRAN response curve. In estimating damping coefficients it is advisable to use transmissibilities derived from sine response tests if possible. In the work discussed here, the sine response test were a much more accurate indication of damping distribution through the structure.

Instrumentation appears to be affecting our ability to correlate the test data with the analytical results. The computed strain in the PWB is larger than the test data and the computed strain in the substrates is lower than the test data. Preliminary computational runs indicate that the accelerometer may be contributing stiffness to the test specimen which was not anticipated in the model. This could lead to the systematic discrepancies noted above. Adequate modeling allowance for the accelerometer may improve the correlation further.

The current work suggests that a reasonable strategy exists for developing models of complex electronic equipment. That strategy will give accurate predictions of structural performance (stress, deflection, etc.) and will correlate well with test data. The strategy includes:

1) Be rigorous in modeling attachments and connections.

2) Be rigorous in constraints and supports.

3) Use handbook values for stiffness and mass properties of materials.

4) Complex features need to be carefully modeled. Either use rigorous geometric and material properties or accurately calculation properties for simplified models. Be meticulous with composites (printed wiring boards).

5) Apply damping to the highly damped portions of the structure only. Be guided by test data, if it is available.

6) Include instrumentation features in the model if test correlation is desired.

These notes on a modeling strategy are not intended to replace the judgement of an experienced engineer. Rather, it is hoped that it will encourage analysts since the careful application of their skills can now achieve valuable results in electronics assemblies.

CONCLUSION

Complex electronic structures are constructed from a wide variety of materials. Traditional modeling techniques are adequate for distributing stiffness and mass throughout a model but are not adequate for distributing damping. Recent releases of MSC/NASTRAN make it possible for analysts to control and specify the distribution of damping in the model via structural damping coefficients on the MAT1 cards (which can now be used in all the modal response solutions as well as the direct response solutions). This development allows much more accurate calculation of dynamic responses in complex structures than was previously possible.

The author wishes to thank Mr. Jerrard A. Joseph of the McNeal-Schwendler Corporation for developing the alter described above which greatly facilitated this work.

TABLE I: STRUCTURAL MATERIALS

Applications	Material
Printed Wiring Board	Glass Reinforced Polyimide with 2 oz. Copper Conductor Layers
Connector Shell	6061-T6 Aluminum
Stiffener	6061-T6 Aluminum
Ceramic Substrate	High Alumina Ceramic
Wedge-Lok Clamps	6061-T6 Aluminum
Substrate Solder Pins	Phosphor Bronze
Solder	Lead-Tin Eutectic

TABLE II: TEST RESULTS SUMMARY

Input Accel PSD, g**/Hz (100-2000 Hz.)	.10	.40	1.60
Input Accel., gRMS	13.9	27.8	55.2
Accelerometer Response, gRMS	90.6	140.	226.
01 Strain Gauge Response, x10E+6	68.8	85.2	187.
02 Strain Gauge Response, x10E+6	25.6	59.7	110.
03 Strain Gauge Response, x10E+6	33.9	76.3	161.
04 Strain Gauge Response, x10E+6	111.	179.	435.

TABLE III: MODEL VARIATION EFFECTS

		SOLDER PINS			PWB & SUBSTRATES
	Test Data	Ortho Shells	Straight Bars	Bent Bars	Tailored Element Sizes
Acceleration (RMS)	1.0	1.00	1.00	1.00	1.00
01 Strain Gauge (RMS)	1.0	1.97	2.87	3.37	3.17
02 Strain Gauge (RMS)	1.0	.41	.69	.79	.78
03 Strain Gauge (RMS)	1.0	.38	.32	.34	.38
04 Strain Gauge (RMS)	1.0	1.19	1.71	1.57	1.91

TABLE IV: DAMPING DISTRIBUTION EFFECTS

	Test Data	PWB	Solder Pins	Wedge-Loks	Test Conn.	Card Conn.	Sold P. & C/C	W/L & C/C
Accelerometer (RMS)	1.0	1.0	1.0	1.0	1.0	1.0	1.0	1.0
01 Strain Gauge (RMS)	1.0	3.17	3.28	3.21	2.31	1.15	3.19	3.16
02 Strain Gauge (RMS)	1.0	.78	.78	.74	.68	.44	.76	.66
03 Strain Gauge (RMS)	1.0	.38	.37	.34	.36	.24	.37	.31
04 Strain Gauge (RMS)	1.0	1.91	2.12	2.07	1.49	.90	2.06	2.00

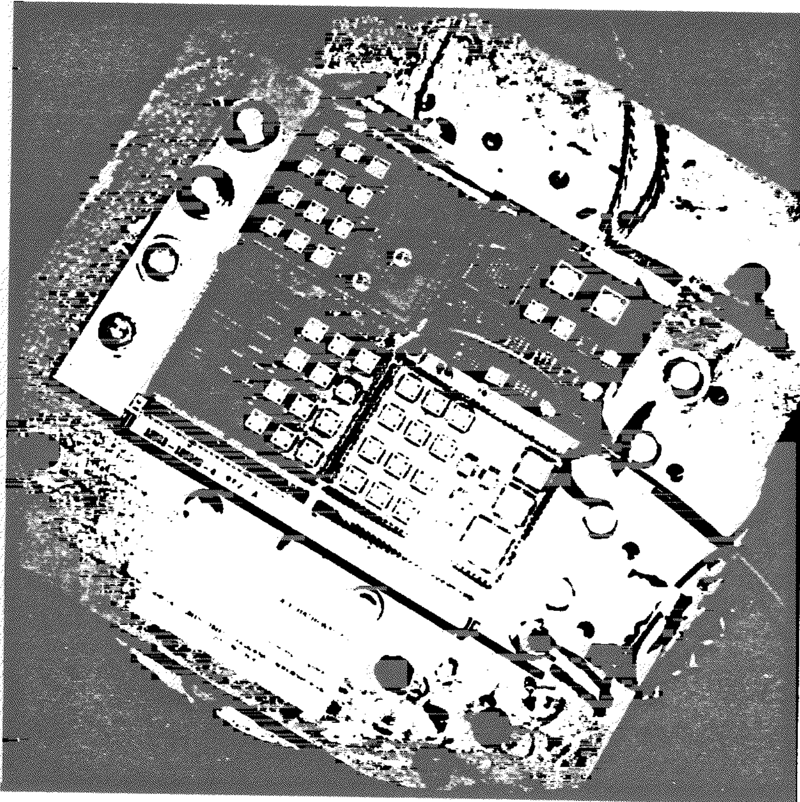

Figure 1. Chip Carriers and Substrates Mounted on a Multi-layer Polyimide Printed Wiring Board.

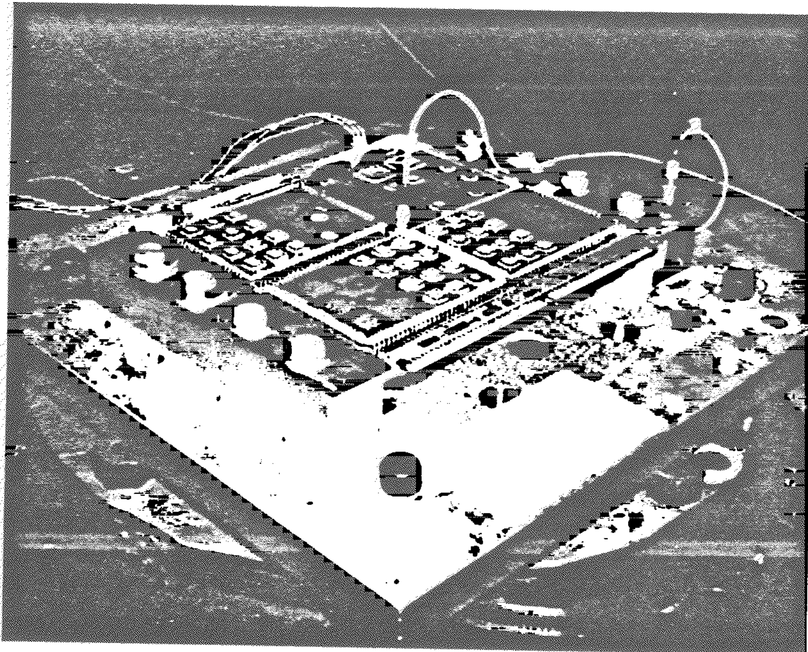

Figure 2. Chip Carrier Assembly Prepared for Random Vibration Testing.

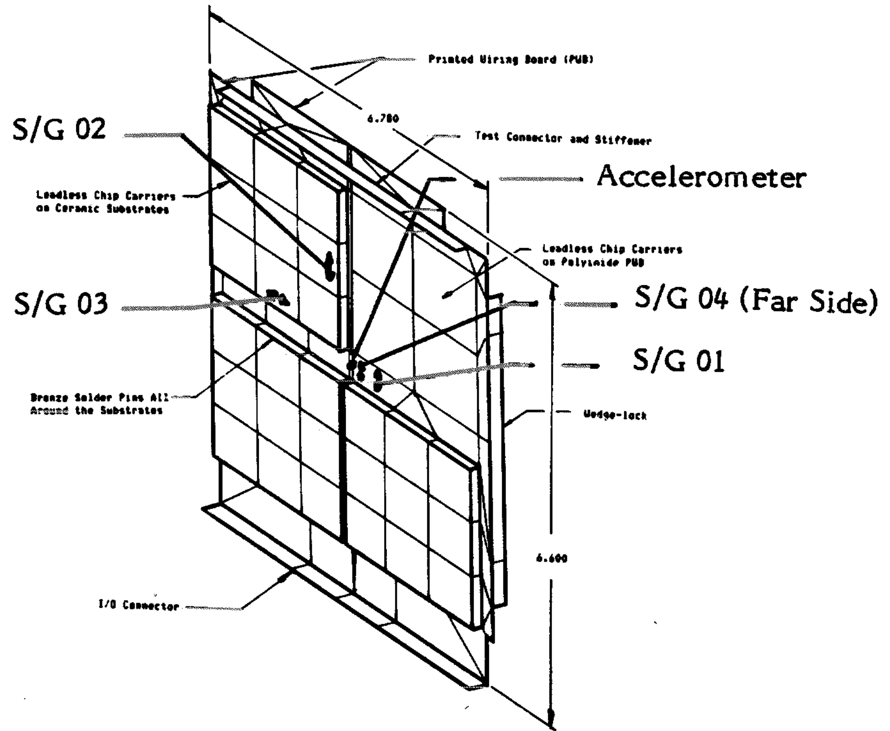

Figure 3. Finite Element Model of Chip Carrier Assembly.

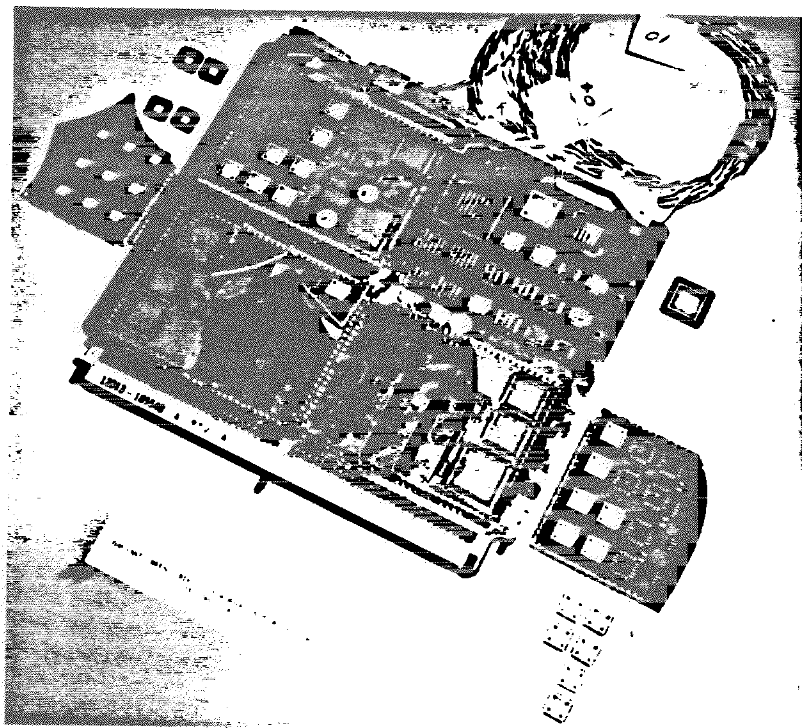

Figure 4. Fractured Speciment after Completion of Tests.

```
ID DAMP ALTER
$
$
$ SET UP TO RESTART DAMPING CHANGES ON MAT1 CARDS.
$
$ FOR USE IN SOL 71, WITH THE MODEL ALL IN THE RESIDUAL STRUCTURE.
$
$ SET UP THE RE-START PROBLEM AS FOLLOWS:
$   EXECUTIVE CONTROL DECK,
$      ADD IN THE ALTER SHOWN BELOW.
$   CASE CONTROL DECK,
$      SET A=0
$      $SEALL=A          (DELETED)
$      SEMG=A            (ADDED)
$      SEMR=A            (ADDED)
$      $METHOD=B         (DELETED)
$      $DYNRED=C         (DELETED)
$   BULK DATA DECK,
$      PARAM,NEWDYN,-1   (ADDED)
$      PARAM,NOTRED,-1   (ADDED)
$
$
SOL 71
TIME 60
DIAG 8,13,19
$
$ BEGIN ALTER
ALTER 180,181
ALTER 682,682
DBFETCH/GOAQ,GOAT,,,/MODEL/SEID/0/DBSET3 $
DBFETCH   /MLAA,KLAA,,,/0/0/0/DBSET3 $
DBSTORE  MLAA,KLAA//SOLID/SEID/DBSET2$
ADD GOAT,GOAQ/GOA $
DBSTORE  GOAQ,GOAT,GOA//SOLID/SEID/DBSET1$
ALTER     718,719
ALTER     828,828
DBFETCH   /GOAQ,GOAT,,,/MODEL/SEID/0/DBSET1$
ADD       GOAT,GOAQ/GOA$
DBSTORE   GOAT,GOAQ,GOA//SOLID/SEID/DBSET1$
$ END ALTER
CEND
```

Figure 5. MSC/NASTRAN Alter Used for Damping Restarts.

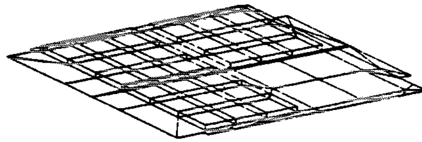

(a) Original Geometry

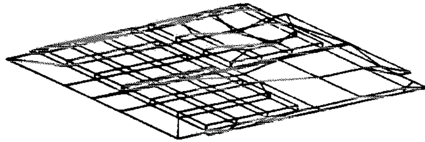

(b) Revised Geometry

Figure 6. Revisions to Shell Elements Near Strain Gage Locations.

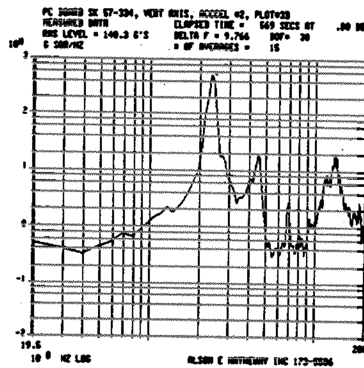

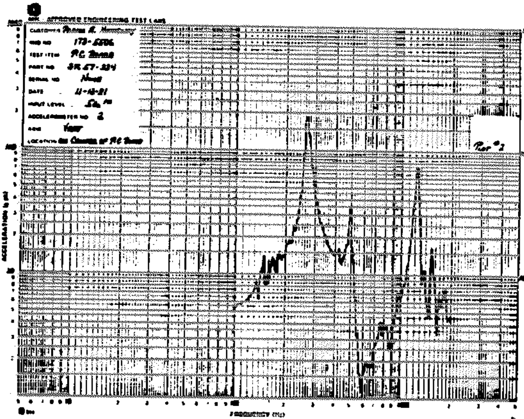

Figure 7. Comparison of Random and Sinusoidal Test Specimen Responses. Top, Random (.04g^2/Hz.); Bottom, Sine (5.0g)

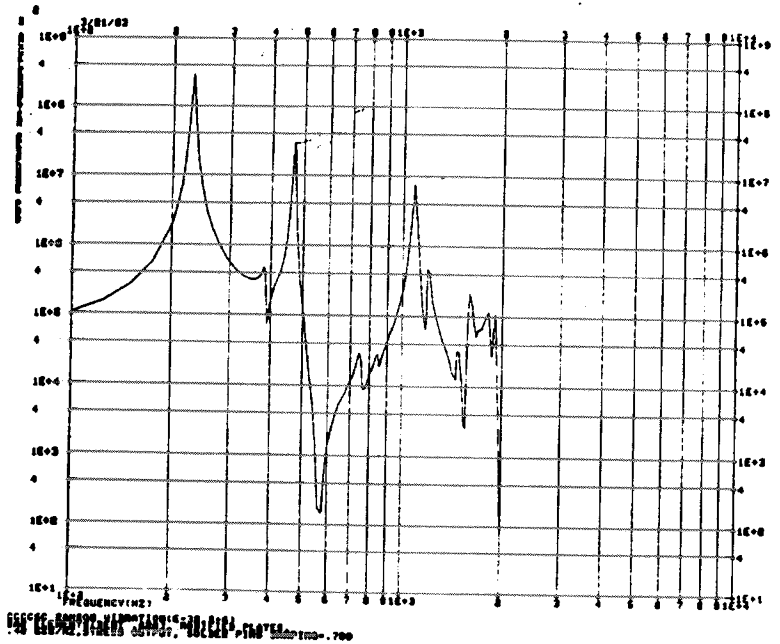

Figure 8. MSC/NASTRAN Random Response Curve.